EUROPHYSICS LETTERS 15 July 2003

Europhys. Lett., **63** (2), pp. 220–225 (2003)

A schlieren method for ultra-low–angle light scattering measurements

D. Brogioli, A. Vailati and M. Giglio

Dipartimento di Fisica and Istituto Nazionale per la Fisica della Materia Università degli Studi di Milano - via Celoria 16, 20133 Milano, Italy

(received 21 March 2003; accepted in final form 16 May 2003)

PACS. 42.25.Fx – Diffraction and scattering.
PACS. 42.79.Mt – Schlieren devices.

Abstract. – We describe a self-calibrating optical technique that allows to perform absolute measurements of scattering cross-sections for the light scattered at extremely small angles. Very good performances are obtained by using a very simple optical layout similar to that used for the schlieren method, a technique traditionally used for mapping local refraction index changes. The scattered intensity distribution is recovered by a statistical analysis of the random interference of the light scattered in a half-plane of the scattering wave vectors and the main transmitted beam. High-quality data can be obtained by proper statistical accumulation of scattered intensity frames, and the static stray light contributions can be eliminated rigorously. The potentialities of the method are tested in a scattering experiment from non-equilibrium fluctuations during a free-diffusion experiment. Contributions of light scattered from length scales as long as $\Lambda = 1\,\mathrm{mm}$ can be accurately determined.

Low-angle static light scattering is a powerful tool to investigate the long-wavelength fluctuations that appear in a great variety of important phenomena, like phase transitions and nucleation processes [1, 2], aggregation of colloidal systems [3, 4], and non-equilibrium systems [5]. As the typical length scale Λ increases, the angular range of interest $\delta\Theta = \lambda/\Lambda$ becomes smaller, and this creates unsormountable difficulties stemming from the cramped solid angle of collection for the scattered light, tighter angular definition for the scattering angle, ever-increasing difficulty with stray light that is preferentially scattered at smaller angles, and, finally, main beam diffraction spilling that also piles up at the low-angle scattering end.

In this letter we describe a new technique that allows to overcome most of the above-mentioned difficulties and can be pushed to arbitrary small angles. This technique relies on a detection scheme totally different from the traditional angle-resolved scattering method [6], and based on an optical setup similar to the schlieren imaging technique, traditionally used to map refraction index modulations [7].

The technique belongs to a family of scattering measurement techniques recently introduced, Near Field Scattering (NFS) [8–10]. These techniques allow to measure scattered intensity distributions from the statistical analysis of the intensity modulations due to the random interference of the scattered waves in the near field. In Heterodyne NFS (HNFS) [10], the scattered light is mixed with the transmitted beam that acts as a reference beam. The scattered intensity distribution is then obtained from the two-dimensional power spectrum of

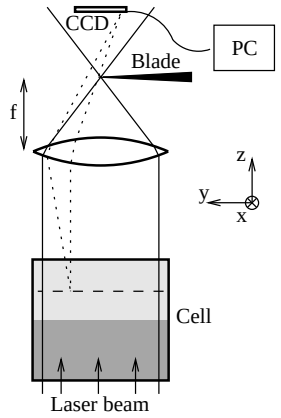

Fig. 1 – The overall instrumental setup. A collimated laser beam is sent through the cell containing two miscible liquids. A lens images a plane inside the cell onto a CCD detector. The transmitted beam is focused by the lens, and the blade cuts half of its waist.

the heterodyne signal falling onto a two-dimensional multielement sensor (a CCD). Indeed, as we will stress later on, for small scattering angles the HNFS becomes a Shadowgraphy technique [11–14]. For transparent samples the transfer function has a wide, pronounced zero around $q = 0$ (as well as multiple zeros at higher scattering wave vectors), and this numbs away the sensitivity where it is mostly sought, namely at extremely small scattering angles. We will show that one of the prominent features of Schlieren-like Near Field Scattering (SNFS) is that its transfer function is flat, irrespective of the investigated wave vector range. We will show that the physical source for the shadow zeros is thus destroyed, and the HNFS method can be restored to arbitrarily small scattering wave vectors.

To show the potentiality of the method, we have applied SNFS to the investigation of non-equilibrium fluctuations arising in a free-diffusion process in ordinary binary mixtures [5]. Non-equilibrium fluctuations scatter light within a very narrow wave vector range in the forward direction, and the scattered intensity decay at large scattering wave vectors follows a simple, steep power law behaviour. Therefore, non-equilibrium fluctuations are an almost ideal test sample to ascertain both the linearity of the response and the q vector range of the method. Although SALS has been effectively used to investigate the non-equilibrium fluctuations in near critical binary mixtures, attempts to use SALS to investigate the fluctuations during free diffusion in ordinary binary liquid mixtures showed that the scattered light is dominated by spurious contributions, due to the main beam diffraction spilling and to the divergence of stray light at small scattering angles. On the contrary, shadowgraph has been successfully used to perform these measurements [13,14]. Unfortunately, shadowgraph sensitivity vanishes for small wave vectors, and also exhibits multiple zeros at higher wave vectors. By contrast, we will show that SNFS transfer function is a constant as a function of scattering wave vector, and it significantly extends the wave vector range of SALS, shadowgraph and NFS techniques. SNFS allows a rigorous subtraction of stray light, without any blank measurement; being a heterodyne technique, it measures the field amplitude, thus providing a wider dynamic range with respect to intensity measurements; also being a self-referencing method, it allows the determination of absolute differential scattering cross-sections.

The optical layout of the system is shown in fig. 1. The output of a 10 mW He-Ne laser is spatially filtered and collimated, so as to obtain a 2 cm diameter beam at $1/e^2$, and sent

through the sample. Let us call $\boldsymbol{k}_0$ the wave vector of the main beam; the goal is to measure $I_\mathrm{s}(\boldsymbol{Q})$, the intensity of the light scattered at wave vector $\boldsymbol{k}_\mathrm{s}$, as a function of the transferred momentum $\boldsymbol{Q} = \boldsymbol{k}_\mathrm{s} - \boldsymbol{k}_0$. A lens with focal length $f = 10\,\mathrm{cm}$ images a plane inside the sample onto a CCD detector with a magnification about 1 (the exact location of the plane is immaterial); the images are made of 512×512 pixels, and are digitized with a dynamic range of 8 bits. The transmitted beam is focused by the lens, and its $3\,\mu\mathrm{m}$ diameter waist is located between the lens and the CCD detector. A blade mounted on an x, z micropositioner is placed perpendicular to the optical axis, so that its edge is in the beam waist. The position of the blade along the optical axis is carefully adjusted so that the blade does not produce diffraction fringes when it crosses the beam. Due to the high sensitivity of the instrument, care has to be taken to avoid even faint airborne disturbances. Therefore, the entire beam path has been shielded with cardboard tubing.

The coordinate system we will use in the following is defined so that the z-axis is the optical axis, and the y-axis is perpendicular to the edge of the blade. Every beam scattered with a negative component of $\boldsymbol{k}_\mathrm{s}$ along the y-axis is focused onto the blade, and thus removed. Since the scattered field is weak compared to the transmitted beam, the intensity $I(x, y)$ is the sum of the strong transmitted beam I_0 and of the small heterodyne term $\delta I(x, y)$, due to the interference between the transmitted and the scattered beams; homodyne terms arising from the interference between the scattered beams can be neglected.

The intensity fluctuation $\delta I(x, y)$ can be decomposed in its Fourier components, with amplitude $\delta I(q_x, q_y)$. A modulation with wave vector $\boldsymbol{q} = [q_x, q_y]$ is generated by the interference of the transmitted beam with the scattered three-dimensional plane wave with wave vector $\boldsymbol{k}_\mathrm{s}(\boldsymbol{q}) = [q_x, q_y, k_z]$ and amplitude $\delta E(q_x, q_y, k_z)$, and therefore $\delta I(q_x, q_y) \propto \delta E(q_x, q_y, k_z)$. In practice, we evaluate the power spectrum $S_{\delta I}(\boldsymbol{q})$, the mean-square value of $\delta I(q_x, q_y)$. This gives the mean intensity of the wave with amplitude $\delta E(q_x, q_y, k_z)$, that is $I_\mathrm{s}(\boldsymbol{Q})$:

$$S_{\delta I}(\boldsymbol{q}) = I_\mathrm{s}[\boldsymbol{Q}(\boldsymbol{q})], \tag{1}$$

where $\boldsymbol{Q}(\boldsymbol{q}) = \boldsymbol{k}_\mathrm{s}(\boldsymbol{q}) - \boldsymbol{k}_0$. Consequently, the scattered intensity can be evaluated by measuring the 2-dimensional power spectrum. Since elastic scattering is considered, k_z is determined by the condition $|[q_x, q_y, k_z]| = k$, with $k = |\boldsymbol{k}_0|$. We can thus easily evaluate the transferred wave vector $\boldsymbol{Q}(\boldsymbol{q}) = \boldsymbol{k}_\mathrm{s}(\boldsymbol{q}) - \boldsymbol{k}_0$:

$$\boldsymbol{Q} = \left[q_x, q_y, k \left\{ 1 - \sqrt{1 - \left(\frac{q}{k}\right)^2} \right\} \right]. \tag{2}$$

If the schlieren blade is removed, both the waves with wave vector $\boldsymbol{k}_\mathrm{s}^+(\boldsymbol{q}) = [q_x, q_y, k_z]$ and $\boldsymbol{k}_\mathrm{s}^-(\boldsymbol{q}) = [-q_x, -q_y, k_z]$ generate fringes with wave vector $[q_x, q_y]$. This leads to the shadowgraph method, where the power spectrum of the image, $S_{\delta I}(\boldsymbol{q})$, shows deep modulations, and even vanishes for some values of q [11,12]. This is due to the fact that the modulations, generated by the interference of the waves scattered at symmetric angles with the main beam, sum up in counterphase. This effect is always present at small wave vectors also for the heterodyne NFS [10]. In SNFS the zeroes are eliminated.

In order to fully appreciate the potentialities of the method, we must remind that NFS techniques are based on the fact that each point of the CCD sensor is hit by light scattered at each scattering angle. This imposes some constraints on the transverse dimension d of the scattering volume and its distance Z from the sensor. In the actual setup of fig. 1, Z represents the distance of the sample from the plane, close to the sample, which is imaged by the lens onto the CCD detector. Each point of the sensor collects light scattered at angles

$\vartheta < \vartheta_{\max}$, where $\vartheta_{\max} = d/Z$. The condition $Z \leq d/\vartheta_{\max}$ represents the Near Field Condition (NFC) [8–10].

In principle, a close distance between the sample and the sensor guarantees the access to a wide range of scattering angles without having to use samples with large spatial extension. However, as we will show shortly, this condition cannot be met for all the NFS techniques, while for SNFS the distance Z can be pushed to zero. When $Z = 0$, the sample is imaged onto the CCD detector. Indeed, other NFS techniques impose a requirement on the minimal distance between cell and sensor. As an example, in the HNFS technique this is due to the fact that waves scattered at wave vectors $\boldsymbol{k}_{\mathrm{s}}^{+}$ and $\boldsymbol{k}_{\mathrm{s}}^{-}$ generate fringes with the same spacing when they interfere with the transmitted beam onto the sensor. When $Z = 0$, the phase difference of the two waves is π, irrespective of the wave vector. Therefore, the superposition of the two interference patterns shifted by π gives rise to a flat intensity distribution at $Z = 0$. In order for the fringes to become visible, one can either block one of the scattered waves, as in the schlieren technique described in this letter, or let the beam propagate, so that a Z-dependent phase shift is introduced. This second solution gives rise to the shadowgraph technique, where the contrast of the fringes is modulated by the distance Z [11, 12]. When Z is large enough to guarantee that the waves scattered at $\boldsymbol{k}_{\mathrm{s}}^{+}$ and $\boldsymbol{k}_{\mathrm{s}}^{-}$ come from non-overlapping regions of the sample, the contrast of fringes ceases to depend on Z and q, because the phase difference between the scattered waves becomes random. This occurs when the diffraction aperture of the sensor $Z\lambda/L$ onto the sample becomes larger than the sensor size L, $Z > L^2/\lambda$ [10]. This condition is not required by the SNFS technique, where arbitrarily small distances and sample sizes can be used, provided that the NFC is satisfied. This shows the great potentialities of SNFS, where by using distances of the order of a few millimeters, a very compact instrument can be obtained. Such a small setup could be very useful in many applications where size is an issue, such as experiments under microgravity conditions, medical apparatus, and *in situ* monitoring in general.

We turn now to the non-equilibrium fluctuations data. Non-equilibrium fluctuations have been investigated by different experimental techniques, and the results so far seem to confirm the theoretical expectations (see ref. [15]). The fluctuations arise whenever there is a macroscopic gradient across the system. A simple way to build up a concentration gradient is to carefully layer two miscible liquids one on top of the other, as is customarily done in a classic free-diffusion experiment.

Let us briefly remind the theoretical expectations for the scattered intensity distribution from a layer of concentration gradient ∇c. The power spectra show a fast q^{-4} power law decay at long wave vectors, and a saturation at a constant value at small wave vectors. The coupling of velocity fluctuations with concentration fluctuations accounts for the q^{-4} decay of the power spectrum at the longer wave vectors. Gravity is responsible for the damping of small wave vector fluctuations.

The roll-off wave vector q_{ro} where the transition occurs is

$$q_{\mathrm{ro}}(t) = \left[\frac{\beta g \nabla c(t)}{\nu D}\right]^{1/4}, \tag{3}$$

where g is the gravitational acceleration, ν is the kinematic viscosity, D is the diffusion coefficient and ∇c is the largest concentration gradient along the cell at time t.

For wave vectors smaller than q_{ro}, the scattered intensity saturates to

$$\frac{I_{\mathrm{s}}(q \longrightarrow 0)}{I_0} = \frac{K_{\mathrm{B}}T}{8\pi^2\rho\beta g}k^4\left(\frac{\partial n}{\partial c}\right)^2 \Delta c, \tag{4}$$

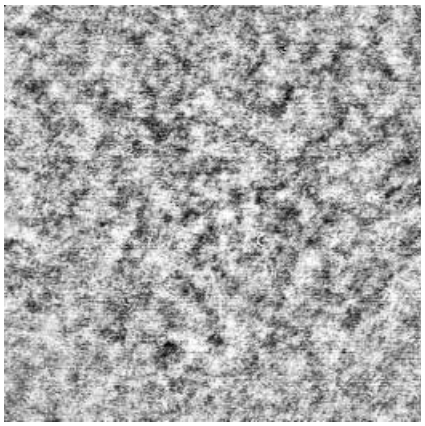

Fig. 2

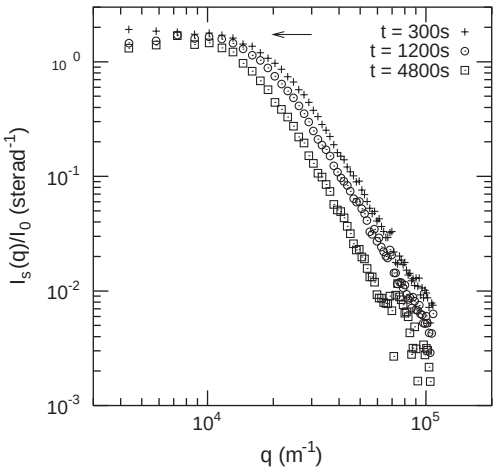

Fig. 3

Fig. 2 – Image of the non-equilibrium concentration fluctuations during the free diffusion of urea in water. The image was recorded 10 minutes after the start of the diffusion process. The side of the image is 4 mm in real space.

Fig. 3 – Relative scattered intensity due to the non-equilibrium fluctuations in the free-diffusion process.

where ρ is the mass density, $\beta = \rho^{-1}(\partial\rho/\partial c)_{p,T}$ is the solutal expansion coefficient and I_0 is the intensity of the main beam.

The measurements have been taken on a water-urea sample, the same system used in refs. [13, 14], where a shadowgraph technique was used. We report in fig. 2 a schlieren image of the fluctuations and in fig. 3 the power spectra obtained at different times during the free-diffusion process. Each curve was obtained by taking the average over typically a hundred images taken over two hundred seconds, and static stray light was accounted for by subtracting the average intensity from each image, as done for the heterodyne method [10]. The potentiality of the method can be best appreciated by comparing the curves in fig. 3 with the ones shown in fig. 3 of ref. [13] and obtained with a shadowgraph method. The improvement is very obvious. The wave vector range for the shadowgraph data is well below a decade, while for the schlieren data it covers a factor of forty between $q_{\min}$ and $q_{\max}$. The shorter range for the shadowgraph method is the result of the confinement between the low-q wide instrumental zero, and the tight sequence of zeros at larger wave vectors. No such a limitation exists for the schlieren method, where the instrumental transfer function is flat. In spite of the moderate dynamic range (two decades), the shadowgraph data appear noisy. At variance, as can be easily appreciated from fig. 3, the schlieren data show little noise over a range of almost one thousand in the scattered intensity. Incidentally, this method profits on the huge number of pixels, leading to a statistical accuracy well beyond the intrinsic 8-bit dynamic range of the frame grabber. The overall improved quality of the data permits a fairly good estimate of the roll-off wave vector. As time goes on, the concentration gradient ∇c decreases as $t^{-1/2}$, and, consequently, $q_{\mathrm{ro}} \propto t^{-1/8}$. Consistently with this, when the time t is increased by 16 times from the first measurement to the last, q_{ro} is reduced by about a factor $1.4 \approx 16^{1/8}$.

Finally, eq. (1) can be used to calculate, with no adjustable parameters, the absolute value of the scattered intensity at $q = 0$, as from eq. (4). An arrow in fig. 3 indicates the no-adjustable-parameter estimate for $I(q \to 0)$. As can be noticed, the agreement is very good.

In conclusion, we feel that the schlieren method described in the present work could be of great interest in performing extremely low-angle light scattering experiments that are of interest for large-scale aggregation processes, nucleation and growth phenomena on length scales that will merge very naturally into regimes that traditionally are covered by more classical methods, like interferometry. The compactness of the layout may prove an asset for tight space requirements like microgravity setups, where the larger-size objects can be conveniently investigated without disturbing sedimentation processes.

* * *

This work has been partially supported by the Italian Space Agency (ASI).

REFERENCES

[1] Stanley H. E., *Introduction to Phase Transitions and Critical Phenomena* (Oxford University Press, Oxford) 1971.
[2] Domb Cyril, *The Critical Point* (Taylor & Francis, London) 1996.
[3] Lin M. Y., Lindsay D. A., Weitz H. M., Ball R. C., Klein R. and Meakin P. A., *Proc. R. Soc. London, Ser. A*, **423** (1989) 71.
[4] Asnaghi Daniela, Carpineti Marina, Giglio Marzio and Vailati Alberto, *Curr. Opin. Colloid Interface*, **2** (1997) 246.
[5] Vailati A. and Giglio M., *Nature*, **390** (1997) 262.
[6] Brogioli Doriano, *Near Field Speckles*, PhD Thesis, Università degli Studi di Cagliari (2001), available at `http://lxmi.mi.infn.it/labgiglio/NFS_PhD/`.
[7] Goodman J. W., *Introduction to Fourier Optics* (McGraw-Hill Book Company, New York) 1968.
[8] Giglio Marzio, Carpineti Marina and Vailati Alberto, *Phys. Rev. Lett.*, **85** (2000) 1416.
[9] Giglio Marzio, Carpineti Marina, Vailati Alberto and Brogioli Doriano, *Appl. Opt.*, **40** (2001) 4036.
[10] Brogioli Doriano, Vailati Alberto and Giglio Marzio, *Appl. Phys. Lett.*, **81** (2002) 4109.
[11] Wu M., Ahlers G. and Cannell D. S., *Phys. Rev. Lett.*, **75** (1995) 1743.
[12] de Bruyn J. R., Bodenschatz E., Morris S. W., Trainoff S. P., Hu Y., Cannell D. S. and Ahlers G., *Rev. Sci. Instrum.*, **67** (1996) 2043.
[13] Brogioli D., Vailati A. and Giglio M., *Phys. Rev. E*, **61** (2000) R1.
[14] Brogioli D., Vailati A. and Giglio M., *J. Phys.*, **12** (2000) 39.
[15] Li W. B., Segrè P. N., Gammon R. W. and Sengers J. V., *Physica A*, **204** (1994) 399.